Examination of chloride ligation in inorganic model compounds relevant

to Photosystem II using Mn X-ray absorption spectroscopy

Shelly A. Pizarro,[†‡] Hendrik Visser,[†‡] Samudranil Pal,[§] Sumitra Mukhopadhyay,[§] Henry J. Mok,[§]

Kenneth Sauer,[†‡] Karl Wieghardt,[¥] William H. Armstrong,[§] and Vittal K. Yachandra*[†]

Melvin Calvin Laboratory, Physical Biosciences Division, Lawrence Berkeley National

Laboratory, Berkeley, CA 94720, Departments of Chemistry, University of California, Berkeley,

CA 94720, and Boston College, Chestnut Hill, MA 02167, and Max Planck Institut für

Strahlenchemie, D-45413 Mülheim an der Ruhr, Germany.

*Corresponding author: Dr. Vittal Yachandra
                        Lawrence Berkeley National Lab
                        1 Cyclotron Rd., Bldg 3
                        Berkeley, CA 94720
                        VKYachandra@lbl.gov
                        Tel: (510) 486-4330
                        Fax: (510) 486-6059

Abstract

Chloride ions are essential for proper function of the photosynthetic oxygen evolving complex (OEC). The specific structural and mechanistic roles of chloride in the OEC remain unresolved. Recent polarized Mn EXAFS studies from our laboratory using oriented Photosystem II membranes in the S_3 state, have provided the first evidence that chloride may be ligated to the Mn cluster of the OEC. This study presents evidence from X-ray Absorption Spectroscopy (XAS) characterizing the Mn-Cl vector in inorganic compounds that are structurally analogous to the proposed model for the OEC. Three sets of model compounds with $Mn^{IV}_3O_4X$ (X = Cl, F, or OH) or $Mn^{IV}_2O_2X$ (X = Cl, F, OH, OAc) core structures were examined using XAS to document changes in the spectra attributable to the Mn-Cl bond. The Mn K-edge energy for compounds containing chloride as a ligand is lower relative to values for structural analogs that have a more electronegative ligand. Fourier transforms (FT) of the EXAFS region reveal a feature near apparent distance R' = 1.7 Å that is present only in compounds where chloride is directly ligated to Mn. These features were isolated and fit with various Mn-X interactions (X = O, N, Cl, F). Simulations using Mn-Cl interactions with a 2.3 Å bond distance provided the best fit, confirming that direct chloride ligation to Mn can be detected in the FT profile of the EXAFS data and is responsible for the observed FT feature at R' = 1.7 Å.

* To whom correspondence should be addressed. Email: VKYachandra@lbl.gov, Fax:

(510)486-6059

† Lawrence Berkeley National Laboratory

‡ University of California

§ Boston College

¥ Max Planck Institut

⊗ Abbreviations: bpea, N, N-bis(2-pyridylmethyl)-ethylamine; EXAFS, extended x-ray absorption fine structure; FT, Fourier transform; IPE, inflection point energy; OAc, acetate ligand; OEC, oxygen evolving complex; PS II, photosystem II; tacn, 1,4,7-triazacyclononane; XANES, x-ray absorption near edge structure; XAS, x-ray absorption spectroscopy; XRD, x-ray diffraction.

Introduction

The oxygen-evolving complex (OEC) of Photosystem II (PS II) is a tetranuclear

manganese cluster that catalyzes the conversion of water into oxygen in a multistep process. The

OEC is driven by light to cycle through five different stages, called S-states (S_0 - S_4), collecting

four oxidizing equivalents before dioxygen is released[1]. X-ray absorption spectroscopy (XAS)

has been a useful tool to directly probe the metal cluster within the PS II membrane protein and

has provided the basis for a working structural model of the OEC.[2,3] As has been the case with

other protein-bound metal centers, the success of gaining structural parameters from the EXAFS

(extended x-ray absorption fine structure) region has encouraged bioinorganic chemists to

synthesize structurally relevant "model complexes".   The corresponding study of the XAS of

inorganic compounds with known structures that mimic elements of the proposed OEC structure

have already proved beneficial in interpreting the PS II data (for reviews see references 4, 5).

The set of compounds that we have chosen for this study aim to clarify the structural role of the

chloride cofactor in PS II.

It has been known for some time that chloride is an essential cofactor in the proper

function of the OEC, but its specific structural and mechanistic roles remain controversial.[6-8]

There is one functional Cl^- per PS II unit,[9] and it is unclear whether it is directly ligated to Mn in

one or more of the five S-states of the oxidation cycle. Studies of the OEC steady-state kinetics

with functional substitutions using Br^- or NO_3^- indicate that Cl^- is closely associated with the

OEC core rather than with the protein matrix and is necessary for the $S_2 \wedge S_3$ and $S_3 \wedge S_0$

transitions of the oxidation cycle.[8-13]

      This study examines the Mn XAS of three sets of inorganic model compounds to

document the structural effect of direct chloride ligation to Mn. All compounds have a Mn^{IV}

oxidation state and have μ-oxo-bridged core structures (Mn_2O_2 or Mn_3O_4) that provide Mn-Mn

distances similar to those reported for the OEC Mn cluster: 2.7 and 3.3 Å. The goal is to

compare the effect of selected ligands on Mn when the oxidation state and the core structure are

maintained. In systematically examining the XAS from different Mn-X interactions (X = Cl, F,

O) within each set of compounds, one can gain structural insight to the configuration of the OEC

Mn cluster. Additionally, the structural parameters gained from the EXAFS of each model

compound can be compared to available x-ray diffraction (XRD) data and validate the accuracy

of the EXAFS method in exposing the atomic interactions in a system where the structure is not

known.

Experimental Section

Sample preparation. The model compounds included in this study were prepared and

characterized in different laboratories. There are two sets of Mn binuclear compounds:

$[Mn_2O_2\mathbf{X}_2(tacn)_2](BPh_4)_2$ where $\mathbf{X}$ = Cl or F,[14] $[Mn_2O_2Cl_2(bpea)_2](ClO_4)_2$ [15] and

$[Mn_2O_2(O_2CCH_3)(bpea)_2](ClO_4)_3$ [16]; and one set of Mn trinuclear compounds:

$[Mn_3O_4\mathbf{X}(bpea)_3](ClO_4)_3$, where $\mathbf{X}$ = Cl, F,[17] or OH[16]. All compounds exhibit the Mn^{IV} oxidation

state, and a schematic of their core structures is presented in Figure 1. For convenience in the text discussion, the compounds are labeled according to number of Mn and differentiating ligand of interest as follows: **Mn$_2$Cl$_2$(t)**, **Mn$_2$F$_2$(t)** for the Mn binuclear compounds containing (tacn) ligands and **Mn$_2$Cl$_2$(b)**, **Mn$_2$OAc(b)** for those containing (bpea) ligands; the Mn trinuclear compounds are labeled as **Mn$_3$Cl**, **Mn$_3$F**, and **Mn$_3$OH**. Samples for XAS measurements were prepared by carefully mixing each model compound with boron nitride in a 1:10 ratio then packing this powder mixture into 0.5 mm thick aluminum sample holders (4 mm x 20 mm) sealed with Mylar windows.

X-ray absorption spectroscopy. XAS data were gathered at beam line 2-3 of the Stanford Synchrotron Radiation Laboratory, operating at 3.0 GeV with beam currents between 70 and 100 mA. A monochromator outfitted with Si<220> crystals detuned to 50% to reject higher harmonics, was used to provide radiation in the 6.4-7.1 keV energy range. Sample temperature was maintained at 10 ± 2 K with a liquid helium cryostat (Oxford Instruments, Bedford, MA). Data were collected as fluorescence excitation spectra using a Lytle detector[18,19] filled with argon gas and placed orthogonal to the incident beam. The fluorescence signal was divided by the incident photon flux detected at the first ionization chamber (filled with N$_2$ gas) to obtain the absorption. Scans were collected from 6520 to 7100 eV, with step sizes of 0.2 eV in the XANES region (6535 to 6575 eV) and 0.5 Å^{-1} in the EXAFS region (k = 2 to 12 Å^{-1}). Energy calibration

was achieved by reference to the position of the maximum pre-edge XAS feature from $KMnO_4$

(6543.3 eV, FWHM ≤ 1.7eV) taken simultaneously. Two to eight scans were averaged for each

sample.

XAS data analysis. The method of data preparation for XANES and EXAFS analysis has been

previously documented[20-22] and is briefly summarized here. For each sample, all measured

absorption scans were calibrated and then combined to improve signal-to-noise. The pre-edge

background was fitted to a straight line and subtracted from the spectra. The data were then

divided by the Mn free-atom absorption and normalized to unity at the absorption edge by

extrapolating a quadratic line fit from the post edge region (>7000 eV) to intersect with the rising

edge. The K-edge energy position was deduced by two different methods: (1) a calculation of

the first moment or mean energy of the rising edge, μ(E), according to

$$\langle E \rangle = \frac{1}{\mu_2 - \mu_1} \int_{\mu_1}^{\mu_2} E(\mu) d\mu$$

where E(μ) is the inverse function of the absorption and μ_2 and μ_1 are the limits of the

normalized absorption intensity range, and (2) the inflection point energy (IPE) of the main

absorption edge as determined from the first zero-crossing of its second derivative. In the first

moment calculation, the integration limits were chosen as 0.15 and 1.0 of the normalized

intensity so that the pre-edge and post-edge absorption regions would not be included. For the

IPE method, analytical differentiation of the absorption edge utilized a third-order polynomial fit over a region of specified length. The data were subjected to differentiation intervals of 5 eV ($\pm$ 2.5 eV from each data point) and 2 eV ($\pm$ 1.0 eV) to assess the variability in the IPE value due to the size of the differentiation interval.

For analysis of the EXAFS region, an initial background removal was performed by fitting a quadratic or polynomial line to the post edge region and subtracting it from the spectra. As described in Cinco *et al.*,[20] the resulting spectra were then converted into a photoelectron wave vector denoted as 'k-space' and weighted by k^3. A spline function was subtracted prior to performing a Fourier transform (FT). The FT contains peaks appearing at R' = (R + Ψ/2) representing scatterers at average distance <R> from Mn. Due to the phase shift, the apparent distance R' is generally less than <R> by 0.2 - 0.5 Å. Typically, we observe incomplete background removal of low-frequency noise indicated by a small peak with R' < 1 Å, and spline functions are chosen to minimize the amplitude of this peak or to maintain a clear separation from the other FT peaks.

The FT peaks at R' > 1 Å were isolated both individually when a clear separation is possible and in groups, and were back-transformed for fitting to single-scattering amplitude and phase functions calculated using the program FEFF 5.05.[23,24] The crystal structure coordinates of a representative compound from each core set of compounds were used to calculate the FEFF

functions used in the least-squares curve fitting of the isolated FT peaks. The fit extracts four

parameters: R, N, σ^2 and ΔE_0, where N represents the number of scatterers (per Mn) at distance

R, σ^2 is the Debye-Waller term, and ΔE_0 is the difference between the ionization threshold E_0 of

the reference and of the unknown. Effort was made to keep fit parameters R ($\pm$ 0.05 Å) and N

($\pm$ 25%) close to the observed crystallographic values of each compound where available. A

single ΔE_0 was used in multiple scatterer fits, and σ^2 was restricted ($0.001 < \sigma^2 < 0.025$) to

produce accurate N values. The quality of the fit was judged by the sum of residuals between the

simulation and the experimental data multiplied by the k-space weighting factor k^3, (error

parameter 'Φ' described in reference 20) as well as by close agreement with the XRD values.

Results

Mn X-ray Absorption Near Edge Structure (XANES). The Mn K-edge absorption spectra of

all three sets of compounds is presented in Figure 2 while their respective second derivatives are

shown in Figures 3A and 3B. Table 1 contains the Mn K-edge absorption energy values derived

from the XANES spectra. The absorption of the first set of binuclear Mn compounds, **Mn₂Cl₂(t)**

and **Mn₂F₂(t),** is nearly identical for both compounds in the pre-edge region and then begins to

diverge at 6545 eV. The second derivative of the **Mn₂Cl₂(t)** absorption clearly shows that there

is an inflection point near 6550 eV in its K-edge that is barely discernible in the XANES profile.

This inflection produces a zero-crossing, i.e. an IPE value, that is much lower (~4 eV) than that

of **Mn₂F₂(t)**. The second derivative (Figure 3A-A) of **Mn₂F₂(t)** shows that, although a feature

similar to that seen in **Mn₂Cl₂(t)** is apparent, it does not reach the zero line to become the IPE.

Table 1 shows that the K-edge energy difference, calculated from the first moment <E>, is only

0.85 eV between these two compounds. Both calculation methods have their respective

drawbacks and advantages and, although they do not agree in magnitude, the trend is clearly in

favor of lower K-edge energy for **Mn₂Cl₂(t)**.

The second set of binuclear Mn compounds, **Mn₂Cl₂(b)** and **Mn₂OAc(b)**, have the same

Mn₂O₂ core structure as the **Mn₂(t)** set, but the aromatic terminal (bpea) ligands influence the

overall Mn environment towards a generally lower <E> values. Unlike the first set, there is no

clear pattern in the edge energy values according to electronegativity. Although oxygen is more

electronegative than chloride, the difference is not so great as compared to fluoride, and this can

be seen in the K-edge energy values. The difference in <E> between the two compounds is only

0.18 eV, unlike the **Mn₂(t)** set which compares chloride and fluoride ligands and where the

difference in <E> values was much larger (0.85 eV). The IPE values, taken from the 2 eV

second derivative (Figure 3A-B), would appear to bolster this meager difference in <E> by

providing **Mn₂Cl₂(b)** with an IPE that is 2.5 eV lower than that of **Mn₂OAc(b)**; however, this

zero-crossing feature in **Mn₂Cl₂(b)** is attenuated when using a 5 eV differentiation interval and

the resulting IPE is very close (< 0.1 eV) to that of **Mn₂OAc(b)**. The Mn K-edge is clearly

sensitive to the ligand environment; slight differences in the **Mn₂OAc(b)** structure imposed by

the rigidity of the acetate bridge may interfere with a clear-cut determination of the electronegative contribution from the Cl and O ligands. Because the overall structures of **Mn₂Cl₂(b)** and **Mn₂OAc(b)** are not identical, as they are in the **Mn₂(t)** set, direct comparisons between the edge energy values cannot be so conclusive. This example also demonstrates how difficult it is to reduce the complexity of these absorption edges to a single numerical value.

The Mn K-edge profiles from the set of trinuclear Mn compounds (**Mn₃Cl**, **Mn₃F**, and **Mn₃OH**) presented in Figure 2C show that the amplitude of the pre-edge [1s→3d] transition is noticeably higher for the **Mn₃OH** compound resulting from a distortion in its core structure (observed in the XRD) that brings these orbitals into a more favorable orientation. As for the **Mn₂(t)** set, the Mn K-edge energy of the chloride containing compound (**Mn₃Cl**) is lower than that of **Mn₃F**, in accord with the electronegativities of these two halides. However, the K–edge energy of **Mn₃Cl** and **Mn₃OH** are quite similar; the difference in <E> is 0.11 eV and in IPE 0.03-0.28 eV. Once again, slight changes in the overall structure of these two compounds prevent an accurate quantitation of the effect that Cl and O have on the Mn XANES.

Mn Extended X-ray Absorption Fine Structure (EXAFS). Figure 4 displays the EXAFS region of each model compound weighted by a factor k^3 to compensate for the decay of the EXAFS amplitude at higher k-values; the Fourier transform (FT) for the EXAFS oscillation of each compound is shown in Figure 5. Although the amplitudes for **Mn₂Cl₂(t)** and **Mn₂F₂(t)** are

similar, the different halide ligands influence the phase of the oscillation. This differential offset

in the phase is even more apparent in the set of **Mn$_2$X$_2$(b)** compounds, where even at high

k–values there is an obvious difference in the phase. X-ray diffraction (XRD) measurements

show that the Mn-Mn distance in each of these compounds is noticeably different: 2.76 Å in

Mn$_2$Cl$_2$(b) and 2.58 Å in **Mn$_2$OAc(b)**.[15,16] In addition, the Mn-Cl distance (2.27 Å) in

Mn$_2$Cl$_2$(b) is longer than the average Mn-O distance of the acetate bridge in **Mn$_2$OAc(b)**

(1.94 Å). This significant difference in distance to the nearest neighbor affects the phase of the

interference wave created by the exiting electron, as can be seen in the *k*-space EXAFS profile.

In contrast, the set of trinuclear Mn compounds exhibits EXAFS profiles that are very similar in

both amplitude and phase for all three compounds. Although the Mn-Cl and Mn-OH distances

found in the Mn$_3$X compounds are comparable to those found in the other (bpea) compounds,

Mn$_2$Cl$_2$(b) and **Mn$_2$OAc(b)**, the Mn–Mn separation and consequently the wave vector phases

are more uniform among the three Mn$_3$X compounds.

The Fourier transform of the EXAFS data separates the various interaction waves

according to distance from Mn. Figure 5 shows that chloride-containing compounds have a

unique feature near apparent distance R' = 1.7 Å that is absent or attenuated in all of the other

compounds. Isolating this feature and fitting its back-transformed oscillation (i.e., Fourier

filtering) with Mn-X vectors of known identity and bond length reveals the characteristics of the

interacting ligand. The FT peaks I and II from **Mn$_2$Cl$_2$(t)** are not well separated and so have

been isolated together; the resulting filtered *k*-space EXAFS profile is displayed in Figure 6

along with the best fit simulations of the data. The parameters for these fits are reported in

Table 2. Fit A-1 contains only two interaction shells (Mn-O and Mn-N) to represent the nearest

ligands to Mn, the bridging μ-oxygens and the terminal (tacn) ligands. Figures 6B and 6C show

that Fit A-1 can be greatly improved by the addition of a third interaction shell with a fixed

coordination number of N = 1.0; addition of Mn-O lowers Φ by 36% (Fit A-2, Figure 6B), while

addition of Mn-Cl reduces Φ by 77% (Fit A-3, Figure 6C) and appears at 2.27 Å.

The FT profile of **Mn$_2$Cl$_2$(b)** is not so well-resolved. Once again, there is a peak near

R' = 1.7 Å, but this cannot be cleanly separated from the other features; the entire three-peak

profile has been filtered and is displayed in Figure 7. The fitting parameters for **Mn$_2$Cl$_2$(b)** are

shown in Table 3. The information gathered from XRD is also included in Table 3 and was used

as a starting point in all of the simulations; fitting parameters were intentionally kept close to

these values. A good fit is already obtained starting with a 4–shell simulation representing all

core and terminal ligands except for Cl (Fit B-1, Φ = 0.132 x 10^3). Various Mn-X interactions

with N fixed at 1.0, and an initial distance of 2.1 Å that was allowed to vary, were added to this

4-shell simulation; the best two are presented in Table 3. Visually, the 5-shell simulations

including either a Mn-O or a Mn-Cl interaction shell are difficult to differentiate (Figure 7).

However, the improvement in Φ shows that Mn-Cl (Table 3, Fit B-3, Δ(Φ) = -34%) is a better

choice than Mn–O (Fit B-2, $\Delta(\Phi)$ = -20%). The Mn-Cl distance obtained from the fit is 2.21 Å

and is comparable to that measured through XRD (2.273 Å).

Lastly, the FT profile of the **Mn₃Cl** compound (Figure 5) shows a shoulder near

R' = 1.7 Å, and this was isolated along with the first peak. An initial 2-shell simulation (Table 4,

Fit C-1) is improved by adding a third interaction shell with N = 0.3 (Figure 8). Adding the

Mn–Cl interaction greatly improves the 2-shell simulation ($\Delta(\Phi)$ = -42%), whereas a Mn-O

interaction shell at a similar distance is only marginally better ($\Delta(\Phi)$ = -7%). Once again, the

Mn-Cl distance gained from the fit (2.30 Å) is close to that observed in XRD (2.242 Å).

Visually, the overall fit of this final simulation is not so satisfying as that of the other two

compounds, and improvement can be gained if the fitting parameters are relaxed beyond the

narrow constraints we have imposed using the XRD values. Such simulations give the same

general result, namely that the Mn-Cl vector is significantly superior to the alternative Mn-O at

R ~2.2 Å, but the coordination numbers and interatomic distances of each Mn-X interaction

differ significantly from those of the XRD.

Discussion

Mn XANES. Because XANES records a 1s^4p absorption transition (K-edge), the Mn

absorption edge is sensitive to both oxidation state and surrounding ligands. All of the

compounds chosen for this study have an oxidation state Mn^{IV} and have been separated into three

14

sets according to the number of Mn and the nature of the terminal ligand group. With the Mn

oxidation state kept constant, the effect of the surrounding ligands on the Mn absorption edge

can be evaluated. One of the quantitative measures that is typically reported for K-edge spectra

is the energy at which the transition takes place. In this study we have used two methods to

calculate this so called 'edge energy' to call attention to the subjectivity of this measurement and

the difficulty of using a single numerical value to represent the k-edge absorption. The first and

more extensively used method is to measure the inflection point energy (IPE) from the first zero-

crossing observed in the calculated second derivative function of the main absorption edge.

Although it is qualitatively adequate to compare the second derivatives of two compounds, the

drawback of this method is its insensitivity to structure within the K-edge when the energy

window chosen for differentiation is too wide. Subtle structure within the K-edge is accentuated

in its second derivative and, according to the energy interval chosen for differentiation, the

position of the zero-crossing changes. The second method used for calculating the edge energy

integrates the area underneath the absorption edge curve within specified limits to obtain the first

moment <E> labeled as the mean energy. This method is much less sensitive to changes in the

shape of the K-edge, however, it is strongly dependent on the limits of integration and reduces

the edge structure to a single numerical value. To maintain an equal evaluation of all of the main

absorption edges, the limits were arbitrarily chosen to be 0.15 and 1.0 of the normalized

absorption edge rise following the method described in Iuzzolino *et al.* [25] This chosen segment

minimizes the contribution from both the pre–edge absorption and that of post-edge states.

Table 1 reports all Mn K-edge energies calculated from both the mean energy <E> method and the IPE second derivative values taken at two different differentiation widths (2 eV and 5 eV).

Although all of the model compounds in this study have the same formal Mn[IV] oxidation state, the variations seen in the Mn XANES show that the K-edge is sensitive to changes in the effective potential of the Mn that are induced by the electron donating character of the ligating atoms[26]. This effect is best observed for two structurally analogous Mn compounds with different halide ligands. The greater electronegativity of the F ligand draws electrons away from the Mn[IV] core and therefore shifts the K-edge absorption towards a higher energy compared to that for a Cl ligand. The difference in <E> between **Mn$_2$Cl$_2$(t)** and **Mn$_2$F$_2$(t)** is 0.85 eV (Table 1), while in the set of trinuclear Mn compounds (**Mn$_3$Cl** vs. **Mn$_3$F**) it is 0.5 eV. Although different in magnitude, the IPE values also show a similar pattern that distinctly places the compounds containing fluoride at a higher IPE than those containing chloride ligands. This trend is consistent with previous observations made on tetranuclear Mn cubane compounds containing a single Cl or F ligand directly ligated to three of the four Mn[20]. Thus, the two measures, <E> and IPE, show qualitatively similar behavior for distinguishing F and Cl ligands.

By contrast, the comparison between Cl and O ligands is not clearly ordered according to electronegativity. As noted in the Results section, the structural changes imposed by an acetate bridge in the case of the **Mn$_2$OAc(b)**, and hydrogen bonding in **Mn$_3$OH**, affect the position of

the K-edge energy; these values do not directly correlate with those of their chloride-containing

analogs. Such subtle structural changes in the surrounding ligand environment of the Mn have a

complex effect on the observed XANES. Although not plotted together, the variations in the K-

edge profiles (accentuated in the second derivative) between the two sets of binuclear Mn

compounds show that the terminal ligand environment (tacn vs. bpea) has a powerful effect on

the Mn XANES despite the similarity in the core structure and halide ligand. Aromatic ligands

have unoccupied π^* orbitals which can have a strong π back-bonding interactions with the Mn d-

orbitals. The shape of the absorption K-edge is remarkably different for **$Mn_2Cl_2(t)$** and

$Mn_2Cl_2(b)$, and the calculated edge energy for the binuclear Mn compounds containing the

aromatic (bpea) ligands is generally lower than that of the (tacn) compounds.

Lastly, the XANES region can be affected not only by the covalency but also by the

symmetry of the metal center.[27,28] Insensitive to changes in the valence environment of the metal,

the 'forbidden' 1s→3d pre-edge (XANES < 6550 eV) transition has an IPE that appears at the

same position (6539.7 eV) in all of the compounds, and its amplitude is reflective of changes in

the symmetry of the Mn environment. Both sets of binuclear Mn compounds have

correspondingly identical pre-edge features, but in the set of trinuclear Mn compounds the

amplitude of the **Mn_3OH** pre-edge is noticeably higher than that of the other compounds. This

change in the symmetry of the metal center is confirmed by XRD measurements,[16] which show

that there is hydrogen bonding between the OH group and the oxygens bridging the Mn,

resulting in a slight distortion of the core structure to bring better overlap between the electronic orbitals.

Further study of model compounds is needed to fully understand the nature of the substructures seen in absorption K-edges and to solidify correlations between small differences in chemical structure and observed spectra. Although a starting guideline, IPE and <E> values loose sight of the details in the edge profile and cannot be used simply without further consideration of the chemical structure.

Mn EXAFS. The EXAFS region of the Mn absorption profile reveals structural information. The outgoing photoelectron from Mn interacts with its neighboring atoms to produce a scattering pattern that can be analyzed for identity and distance of the neighboring ligands to Mn.[3,29] The sets of compounds chosen for this study address the structural role of the chloride cofactor in PS II. Within each set of compounds, the chloride-containing compound is distinguished by a peak in the FT profile (Figure 5) near apparent distance R' = 1.7 Å that is absent or greatly subdued in the non-chloride containing compounds. The XRD measurements of **Mn₂Cl₂(b)** and **Mn₃Cl** show that the Mn-Cl bond is comparatively longer than the Mn-F and Mn-OH bonds in **Mn₂F₂(b)**, **Mn₃F** and **Mn₃OH**.[15,17] This long bond distance separates the Mn-Cl interaction from the other shorter bond distances (Mn-O and Mn-N) and appears in the FT profile as a distinct shoulder or peak. Fourier filtering of these features and fitting in *k*-space with simulated phase

and amplitude functions of known interatomic interactions and distance allows us to assign these features to Mn-Cl interactions.

Because crystallographic structures are available for **Mn$_2$Cl$_2$(b)** and for **Mn$_3$Cl**, the results of the XRD measurements are included in Tables 3 and 4 for comparison to the EXAFS fit simulations. The results from the two methods are in good agreement. In the best fit for each compound, the coordination numbers are within 25%, while the largest difference in bond distances is 0.063 Å. This gives us confidence that the resulting fit simulations for the **Mn$_2$Cl$_2$(t)** EXAFS are accurate and that the observed peak at R' = 1.7 Å is indeed due to a Mn-Cl interaction in each compound.

The phase and amplitude functions used in the fitting procedure were calculated using the coordinates for a representative model compound with the same core structure. Therefore, the binuclear Mn compounds were fit using a slightly different set of wavevectors from those used for the trinuclear Mn compounds. This implicitly assumes that we have some idea of the starting point of the structure which guides the iteration procedure to obtain the best fit of the data. Because this is a situation that is not possible for a metalloprotein system like PS II, we attempted fits of the FT peaks near R' = 1.7 Å using simulated functions that were not selected or separated according to core structure. The resulting fits were not so satisfactory, but the underlying result was the same; fits containing a Mn-Cl interaction (at 2.3 Å) were superior to those containing a Mn-O interaction at the same distance and coordination. The characteristic

shape of the Mn-Cl back-scatter function cannot be easily simulated by that of Mn–F or Mn-O, which are difficult to distinguish from each other, and stands out clearly as the best fit in the chloride-containing compounds.

Concluding remarks

This study shows that Mn-Cl ligation can be detected via XAS of a set of Mn compounds that possess the same Mn oxidation state and similar core structures. The XANES data show that comparison of the K-edge energy values of **Mn$_2$Cl$_2$(t)** and **Mn$_3$Cl** to those of their respective structural analogs **Mn$_2$F$_2$(t)** and **Mn$_3$F** shows a detectable decrease in the Mn K–edge energy. However, the comparison between Cl and O is not conclusive, owing to small differences in the structures of **Mn$_2$OAc(b)** and **Mn$_3$OH** compared to the chloride containing compounds. This finding has implications for the interpretation of the OEC XANES data. First, the Cl/Mn atom ratio in the OEC is 1/4,[9] while in these compounds it is 1/1 or 1/3. Thus, the effect of direct chloride ligation within the abundance of Mn-O bonds in the OEC may not be easily detected in the Mn K-edge, although chloride has a somewhat lower electronegativity than oxygen. Second, slight changes among the core structures of the model compounds have an effect on the observed XANES. This means that significant changes in the Mn K-edge energy alone cannot be attributed to changes solely in the Mn oxidation state, but can be the result of

structural rearrangement due to chloride binding or releasing at different stages of the oxidation cycle.

In the post-edge region, the *k*-space view of the EXAFS profile in each set of model compounds shows that the phase of the oscillations is affected by the longer Mn-Mn and Mn-Cl bond distances found in the chloride-containing compounds. In fact, it may be this longer Mn-Cl bond that allows detection in the FT profile where a peak or shoulder appears near R' = 1.7 Å. Simulations of these features fit best to Mn-Cl interactions with a ~2.3 Å bond distance, and all structural parameters obtained from the EXAFS data are in good agreement with available results from XRD measurements. This validation gives us confidence that interpretation of the PS II EXAFS data is also accurate.

References

1. Kok, B.; Forbush, B.; McGloin, M. *Photochem. Photobiol.* **1970**, 11, 457-475.

2. Yachandra, V. K.; DeRose, V. J.; Latimer, M. J.; Mukerji, I.; Sauer, K.; Klein, M. P. *Science* **1993**, 260, 675-679.

3. Yachandra, V. K.; Sauer, K.; Klein, M. P. *Chem. Rev.* **1996**, 96, 2927-2950.

4. Pecoraro, V. L.; Hsieh, W.-Y. *Met. Ions Biol. Syst.* **2000**, 37, 429-504.

5. Hage, R.; Kerschner, J. *Trends Inorg. Chem.* **1998**, 5,145-159.

6. Homann, P. H. *J. Bioenerg. Biomembr.* **1987**, 19,105-123.

7. Coleman, W. J. *Photosynth. Res.* **1990**, 23,1-27.

8. Wincencjusz, H.; Yocum, C. F.; van Gorkom, H. J. *Biochemistry* **1999**, 38, 3719-3725.

9. Lindberg, K.; Andréasson, L.-E. *Biochemistry* **1996**, 35, 14259-14267.

10. Wincencjusz, H.; van Gorkom, H. J.; Yocum, C. F. *Biochemistry* **1997**, 36, 3663-3670.

11. Sandusky, P. O.; Yocum, C. F. *Biochim. Biophys. Acta* **1984**, 766, 603-611.

12. Yocum, C. F. *Biochim. Biophys. Acta* **1991**, 1059, 1-15.

13. Ono, T.; Nakayama, H.; Gleiter, H.; Inoue, Y.; Kawamori, A. *Arch. Biochem. Biophys.* **1987**, 256, 618-624.

14. Wieghardt reference on synthesis of tacn compounds

15. Pal, S.; Olmstead, M. M.; Armstrong, W. H. *Inorg. Chem.* **1995**, 34, 4708-4715.

16. Pal, S.; Chan, M. K.; Armstrong, W. H. *J. Am. Chem. Soc.* **1992,** 114, 6398-6406.

17. Armstrong and Mok manuscript on synthesis of Mn trimers

18. Stern, E. A.; Heald, S. M. *Rev. Sci. Instrum.* **1979**, 50, 1579.

19. Lytle, F. W.; Greegor, R. B.; Sandatrom, D. R.; Marques, E. C.; Wong, J.; Spiro, C. L.; Huffman, G. P.; Huggins, P. E. *Nucl. Instrum. Meth.* **1984**, 226, 542-548.

20. Cinco, R. M.; Rompel, A.; Visser, H.; Aromí, G.; Christou, G.; Sauer, K.; Yachandra, V. K.; Klein, M. P. *Inorg. Chem.* **1999**, 38, 5988-5998.

21. Latimer, M. J.; DeRose, V. J.; Mukerji, I.; Yachandra, V. K.; Sauer, K.; Klein, M. P. *Biochemistry* **1995**, 34,10898-10909.

22. DeRose, V. J.; Mukerji, I.; Latimer, M. J.; Yachandra, V. K.; Sauer, K.; Klein, M. P. *J. Am. Chem. Soc.* **1994**, 116, 5239-5249.

23. Rehr, J. J.; Mustre de Leon, J.; Zabinsky, S. I.; Albers, R. C. *J. Am. Chem. Soc.* **1991**, 113, 5135-5140.

24. Rehr, J. J.; Albers, R. C.; Zabinsky, S. I. *Phys. Rev. Lett.* **1992**, 69, 3397-3400.

25. Iuzzolino, L.; Dittmer, J.; Dörner, W.; Meyer-Klaucke, W.; Dau, H. *Biochemistry* **1998**, 37, 17112-17119.

26. Kirby, J. A.; Goodin, D. B.; Wydrzynski, T.; Robertson, A. S.; Klein, M. P. *J. Am. Chem. Soc.* **1981**, 103, 5537-5542.

27. Shulman, R. G.; Yafet, Y.; Eisenberger, P.; Blumberg, W. E. *Proc. Natl. Acad. Sci. USA* **1976**, 73,1384-1388.

28. Srivastava, U. C.; Nigam, H. L. *Coord. Chem. Rev.* **1972**, 9, 275-310.

29. Yachandra, V. K. *Methods Enzymol.* **1995**, 246, 638-675.

Table 1. Mn K-edge absorption energy of Mn compounds calculated by first moment method (the mean energy <E>) and from the zero-crossing of the second derivative of the XANES (the inflection point energy or IPE). The IPE for each compound is calculated using two different differentiation interval widths.

Model compound		Mean energy <E> (eV)	Inflection Point Energy [IPE] (eV)	
			Differentiation width	
			2 eV	5 eV
$[Mn_2O_2Cl_2(tacn)_2](BPh_4)_2$	**$Mn_2Cl_2(t)$**	6551.13	6549.79	6549.79
$[Mn_2O_2F_2(tacn)_2](BPh_4)_2$	**$Mn_2F_2(t)$**	6551.98	6553.36	6553.77
$[Mn_2O_2Cl_2(bpea)_2](ClO_4)_2$	**$Mn_2Cl_2(b)$**	6549.55	6547.23	6549.86
$[Mn_2O_2(O_2CCH_3)(bpea)_2](ClO_4)_3$	**$Mn_2OAc(b)$**	6549.73	6549.73	6549.79
$[Mn_3O_4Cl(bpea)_3](ClO_4)_3$	**Mn_3Cl**	6552.03	6551.55	6551.13
$[Mn_3O_4F(bpea)_3](ClO_4)_3$	**Mn_3F**	6552.53	6551.82	6551.96
$[Mn_3O_4OH(bpea)_3](ClO_4)_3$	**Mn_3OH**	6551.92	6551.58	6551.41

Table 2. Parameters obtained from simulated fits of isolated [Mn$_2$O$_2$Cl$_2$(tacn)$_2$](BPh$_4$)$_2$,

Mn$_2$Cl$_2$(t), EXAFS Fourier transform Peaks I-II shown in Figure 5A. Bold-face numbers

indicate parameter values fixed during the fit calculation. % Δ(Φ) shows the improvement to the

residual value Φ relative to fit A-1.

Fit label	Atomic interaction	R (Å)	N	σ^2 (x 10^3)	ΔE_0	Φ (x 10^3)	% Δ (Φ)
A-1	Mn-O	1.79	2.207	**3**	-20	1.07	-
	Mn-N	2.07	3.677	**4**			
A-2	Mn-O	1.79	1.925	**1**	-12.65	0.687	- 36%
	Mn-N	2.04	3.639	**5**			
	Mn-O	2.17	**1.0**	**1**			
A-3	Mn-O	1.77	1.961	**1**	-19.99	0.245	- 77%
	Mn-N	2.0	2.408	**4**			
	Mn-Cl	2.27	**1.0**	3.3			

Table 3. Parameters obtained from simulated fits of isolated [Mn$_2$O$_2$Cl$_2$(bpea)$_2$](ClO$_4$)$_2$,

Mn$_2$Cl$_2$(b), EXAFS Fourier transform peaks shown in Figure 5B. Bold-face numbers indicate

parameter values fixed during the fit calculation. Interatomic distances obtained by XRD

(reference 15) are included for comparison. % $\Delta(\Phi)$ shows the improvement to the residual

value Φ relative to fit B-1.

Fit label	Atomic interaction	R (Å)	N	σ^2 (x 10^3)	ΔE_0	Φ (x 10^3)	% $\Delta(\Phi)$	XRD R (Å)	N
B-1	Mn-O	1.79	2.399	5.8	-20	0.132	-	1.811	2.0
	Mn-N	2.07	3.665	**6.3**				2.033	3.0
	Mn-Mn	2.74	0.862	**2**				2.756	1.0
	Mn-C	2.99	7.688	9.7				2.914	7.0
B-2	Mn-O	1.78	2.251	**6**	-20	0.105	-20%	1.811	2.0
	Mn-N	2.02	2.626	**12**				2.033	3.0
	Mn-Mn	2.75	1.055	**3**				2.756	1.0
	Mn-C	2.98	8.75	9.5				2.914	7.0
	Mn-O	2.09	**1.0**	**2**				[2.273]	1.0
B-3	Mn-O	1.78	1.868	**4**	-20	0.087	-34%	1.811	2.0

Mn-N	2.07	3.065	**9**			2.033	3.0
Mn-Mn	2.74	0.771	**1**			2.756	1.0
Mn-C	2.97	8.75	1.4			2.914	7.0
Mn-Cl	2.21	**1.0**	1.7			2.273	1.0

Table 4. Parameters obtained from simulated fits of isolated [Mn$_3$O$_4$Cl(bpea)$_3$](ClO$_4$)$_3$, **Mn$_3$Cl**, EXAFS Fourier transform peak I shown in Figure 5C. Bold-face numbers indicate parameter values fixed during the fit calculation. Interatomic distances obtained by XRD (reference 17) are included for comparison. % Δ(Φ) shows the improvement to the residual value Φ relative to fit C-1.

Fit label	Atomic interaction	R (Å)	N	σ² (x 10³)	ΔE$_0$	Φ (x 10³)	% Δ(Φ)	XRD R (Å)	N
C-1	Mn-O	1.79	3.109	4.3	-20	0.770	-	1.798	2.7
	Mn-N	2.11	3.615	**3.5**				2.075	3.0
C-2	Mn-O	1.79	2.750	**3**	-20	0.716	-7%	1.798	2.7
	Mn-N	2.10	3.525	**4**				2.075	3.0
	Mn-O	2.18	**0.3**	**1**				[2.242]	0.3
C-3	Mn-O	1.78	2.546	1.8	-20	0.443	-42%	1.798	2.7
	Mn-N	2.08	3.695	**6.7**				2.075	3.0
	Mn-Cl	2.30	**0.3**	**1**				2.242	0.3

Figure Captions

Figure 1. Schematic of core structures of Mn compounds:**(A)** binuclear Mn compounds

$[Mn_2O_2X_2(tacn)_2](BPh_4)_2$ where X = Cl or F; **(B)** $[Mn_2O_2Cl_2(bpea)_2](ClO_4)_2$ and

$[Mn_2O_2(O_2CCH_3)(bpea)_2](ClO_4)_3$;. and **(C)** trinuclear Mn compounds $[Mn_3O_4X(bpea)_3](ClO_4)_3$

where X = Cl, F or OH. Compounds are labeled according to the abbreviations used in the text

discussion. Only bridging ligands to Mn are shown in the core structure, terminal ligands are

shown separately in the inset boxes.

Figure 2. Normalized Mn K-edge X-ray absorption near-edge structure (XANES) spectra of

compounds: **(A)** $[Mn_2O_2X_2(tacn)_2](BPh_4)_2$ where X = Cl or F; **(B)** $[Mn_2O_2Cl_2(bpea)_2](ClO_4)_2$ and

$[Mn_2O_2(O_2CCH_3)(bpea)_2](ClO_4)_3$; and **(C)** $[Mn_3O_4X(bpea)_3](ClO_4)_3$ where X = Cl, F or OH.

Figure 3. Second derivatives of the XANES region shown in Figure 2 calculated using a

(A) 2 eV and **(B)** 5 eV differentiation interval. The inflection point energy (IPE) of each

compound (reported in Table 1) was determined from the zero-crossing position of the main

absorption feature.

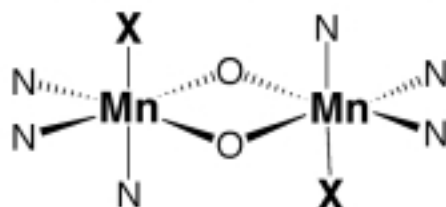**Figure 4.** Background-subtracted k-space Mn EXAFS weighed by k^3.

Figure 5. Fourier transform spectra of *k*-space Mn EXAFS shown in Figure 4.

Figure 6. Fourier filtered *k*-space EXAFS oscillation corresponding to FT peaks I and II of

$[Mn_2O_2Cl_2(tacn)_2](BPh_4)_2$ shown in Figure 5A plotted over simulated Mn-X interactions: **(A)** Fit

A-1 includes 2 interaction shells, while **(B)** Fit A-2 and **(C)** Fit A-3 add a third shell as shown.
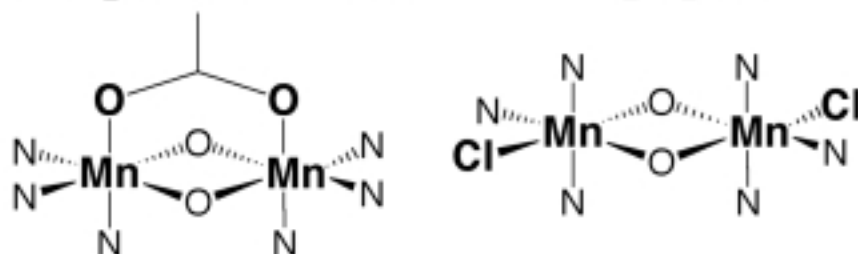
Fitting parameters given in Table 2.

Figure 7. Fourier filtered *k*-space EXAFS oscillation corresponding to FT peaks I, II, and III of

$[Mn_2O_2Cl_2(bpea)_2](ClO_4)_2$ shown in Figure 5B. The data are separately plotted over the two best

fit simulations, and the fitting parameters are given in Table 3 (fits B-2 and B-3).

Figure 8. Fourier filtered *k*-space EXAFS oscillation corresponding to FT peak I of

$[Mn_3O_4Cl(bpea)_3](ClO_4)_3$ shown in Figure 5C. The data are separately plotted over the two best

fit simulations, and the fitting parameters are given in Table 4 (fits C-2 and C-3).

Pizarro et al [**Figure 1**]

(A) Mn₂X₂(t) [X = Cl or F]

(B) Mn₂OAc(b) and **Mn₂Cl₂(b)**

(C) Mn₃X [X = Cl, F or OH]

(tacn) ligand

(bpea) ligand

Pizarro et al **[Figure 3A]**

Pizarro et al **[Figure 5]**

Pizarro et al **[Figure 6]**

A

Mn-O (1.8 Å)
Mn-N (2.1 Å)
Mn-Mn (2.7 Å)
Mn-C (3.0 Å)
Mn-O (2.1 Å)

B

Mn-O (1.8 Å)
Mn-N (2.1 Å)
Mn-Mn (2.7 Å)
Mn-C (3.0 Å)
Mn-Cl (2.2 Å)